Site of Resting State Inhibition of the Nicotinic Acetylcholine Receptor by a Hydrophobic Inhibitor†

David C. Chiara,‡ Marek A. Kloczewiak,§ George H. Addona,§,|| Jeong-A Yu,§,⊥ Jonathan B. Cohen,*,‡ and Keith W. Miller*,§,||

Department of Anesthesia and Critical Care, Massachusetts General Hospital, 32 Fruit Street, Boston, Massachusetts 02114, and Department of Biological Chemistry and Molecular Pharmacology, and Department of Neurobiology, 220 Longwood Avenue, Harvard Medical School, Boston, Massachusetts 02115

Received September 12, 2000; Revised Manuscript Received November 6, 2000

ABSTRACT: The lipophilic photoactivatable probe 3-(trifluoromethyl)-3-(*m*-iodophenyl) diazirine (TID) is a noncompetitive, resting-state inhibitor of the nicotinic acetylcholine receptor (nAChR) that requires tens of milliseconds of preincubation to inhibit agonist-induced cation efflux. At equilibrium, [^{125}I]TID photoincorporates into both the ion channel and the lipid−protein interface of the *Torpedo* nAChR. To determine which of these regions is responsible for resting-state inhibition, we characterized the interactions between [^{125}I]TID and nAChR-rich membranes milliseconds after mixing, by use of time-resolved photolabeling. Photolabeling was performed after preincubation times of 2 ms or 600 s (equilibrium), and the efficiencies of incorporation at specific residues were determined by amino-terminal sequence analysis of nAChR-subunit proteolytic fragments isolated by SDS−PAGE and/or reversed-phase HPLC. Equilibration of TID with lipid was complete within a millisecond as determined by both stopped-flow fluorescence quenching of diphenylhexatriene in lipid bilayers and photoincorporation into nAChR-rich membrane phospholipids. Equilibration with the lipid−protein interface (αM4) was slightly slower, reaching ∼50% that at equilibrium after 2 ms preincubation. In contrast, equilibration with the channel region (αM2 and δM2) was much slower, reaching only 10% that at equilibrium after 2 ms preincubation. Within the ion channel, the ratio of [^{125}I]TID incorporation between M2 residues 9′, 13′, and 16′ was independent of preincubation time. We conclude that TID's access to the ion channel is more restricted than to the lipid−protein interface and that TID bound within the ion channel is responsible for flux inhibition upon activation of the nAChR.

The *Torpedo* nicotinic acetylcholine receptor (nAChR) is the most extensively studied representative of a superfamily of ligand-gated ion channels whose members include muscle and neuronal nAChR, gamma-amino butyric acid receptors (types A and C), glycine receptors, serotonin receptors (type 3), and invertebrate glutamate receptors (*1*). Each receptor is made up of five homologous subunits (∼50 kDa) that associate pseudosymmetrically about the central axis that is the ion channel. Each subunit contains four long stretches of hydrophobic amino acids, three (M1−M3) positioned in the middle of the subunit primary structure and one (M4) at the C-terminus. M2 segments from each subunit contribute to the lumen of the channel while M3 and M4 segments contribute to the lipid−protein interface. The abundance of nAChRs in membranes from *Torpedo* electric organ has enabled both structural determination by cryoelectron microscopy to a resolution of 4.6 Å (*2*) and extensive biochemical and biophysical characterization (reviewed in refs *3* and *4*). nAChRs of *Torpedo* and vertebrate skeletal muscle are made up of four homologous subunits ($\alpha_2\beta\gamma\delta$), with the two agonist binding sites located in the extracellular domain at the α−γ and α−δ subunit−subunit interfaces (*5*).

The nAChR is inhibited by a wide range of noncompetitive antagonists, including local and general anesthetics, many aromatic amines, steroids, fatty acids, and detergents (for review see ref *6*). Such inhibition may occur by several mechanisms. Some noncompetitive antagonists predominantly inhibit the ion channel in the open state by a bimolecular mechanism that probably involves access along the ion permeation pathway and physical occlusion of the lumen of the ion channel. Others act in the absence of agonist either by stabilizing the desensitized state of the receptor or by preferentially interacting with the resting (or closed) state. One example of this latter type of antagonist is the local anesthetic tetracaine, which binds with high affinity within the lumen of the ion channel in the closed state (*7*, *8*). Another example is the lipid-soluble photoreactive-probe

† This research was supported by grants from the National Institute of Health (GM-15904 and GM-58448) and the Massachusetts General Hospital and by an award in Structural Neurobiology from the Keck Foundation. J.-A.Y. was supported by Chosun University.

* Corresponding Authors: K.W.M., phone: (617) 726−8895; FAX: (617) 726−5845; e-mail: k_miller@helix.mgh.harvard.edu and J.B.C., phone: (617) 432−1728; FAX: (617) 734−7557; e-mail: jonathan_cohen@hms.harvard.edu.

‡ Department of Neurobiology, Harvard Medical School.

§ Department of Anesthesia and Critical Care, Massachusetts General Hospital.

|| Department of Biological Chemistry and Molecular Pharmacology, Harvard Medical School.

⊥ Present address: Department of Science Education, Chemistry Major, Chosun University, Kwangju, 501-759, South Korea.

10.1021/bi0021481 CCC: $20.00
Published on Web 12/12/2000

3-(trifluoromethyl)-3-(m-[^{125}I]-iodophenyl) diazirine ([^{125}I]-TID).[1] At equilibrium, TID acts as a potent nondesensitizing, nAChR noncompetitive antagonist (*9*). Quenched-flow measurements of rapid cation efflux from nAChR-rich vesicles indicated that TID is a poor inhibitor when coapplied with the agonist, implying that TID is not an open channel inhibitor (*10*). However, preincubation of nAChR-rich vesicles with TID resulted in an exponential decline in flux response with incubation time, which was reversible and had an observed apparent rate constant of $\sim$10 s^{-1}. Experiments with a fluorescent agonist showed that enhanced fast-desensitization could not account for this observation, leading to the conclusion that TID is a resting state inhibitor. For TID interacting with fetal mouse muscle nAChR, there is also evidence for an open channel component of inhibition (*11*).

Because [^{125}I]TID is a photoreactive reagent whose sites of covalent photoincorporation in the *Torpedo* nAChR have been characterized in great detail, it provides an opportunity to further elucidate the site and mechanism of resting state inhibition. Upon photoactivation, [^{125}I]TID labels all four subunits of the *Torpedo* nAChR (*12*). Two distinct components of photolabeling were distinguished: a specific component, which was agonist-sensitive, inhibitable by classical noncompetitive antagonists, and saturable; and a nonspecific component, which was insensitive to nAChR ligands. The specific component of [^{125}I]TID photoincorporation in the resting state was localized to amino acids on the channel lining surface of the M2 segment from each subunit (*13*), whereas nonspecifically labeled residues in M3 and M4 define the lipid−protein interface (*14*, *15*). Although TID resting state inhibition of the nAChR exhibited a Hill coefficient of one, Wu et al. (*10*) suggested that their kinetic data were consistent with either a single TID binding site or multiple sites of equal affinity. Thus, the inhibitory effects of TID on the nAChR could represent an allosteric effect from the lipid−protein interface association with TID or a direct blockage of the ion channel.

One method to distinguish between these two possible sites of action by TID on the nAChR would be to measure the rates of equilibration at the lipid−protein interface and within the ion-channel and to determine which value corresponds to the rate of resting state inhibition. Recently, a method has been developed that allows large quantities of nAChR-rich membranes to be photolabeled at high yield after exposure to a ligand for times as short as 2 ms (*16*). This work established that [^{125}I]TID photoincorporation into the nAChR-subunits occurred in two phases of nearly equal magnitude. The first phase occurred largely in the deadtime, and the second followed a single exponential with an observed rate of 12−14 s^{-1}. We now use this technique to show that the kinetics of TID access to the M2 ion channel domain are more consistent with the onset of resting state inhibition than are the kinetics of TID equilibration at the lipid−protein interface.

MATERIALS AND METHODS

Materials. nAChR-rich membranes were prepared from *T. californica* electric organ as described (*17*) and stored at −80 °C in 38% sucrose, 0.02% NaN_3. Prior to use, the membranes were pelleted and resuspended in *Torpedo* physiological saline (TPS: 250 mM NaCl, 5 mM KCl, 3 mM $CaCl_2$, 2 mM $MgCl_2$, and 5 mM $NaPO_4$, pH 7.0) at a final protein concentration of 4 mg/mL. [^{125}I]-3-(trifluoromethyl)-3-(*m*-iodophenyl) diazirine ([^{125}I]TID, >10 Ci/mmol) was obtained from Amersham Pharmacia Biotech. TID was synthesized according to the method of Brunner and Semenza (*18*) and stored at −80 °C. TID was diluted into various concentrations in TPS within a few minutes of use. The final ethanol concentration was ≤3.4 mM. We obtained 1,2-dioleoyl-phosphatidylcholine (DOPC) and 1,2-dioleoyl-phosphate (DOPA) from Avanti Polar Lipids, cholesterol (Chol) from Calbiochem, 1,6-diphenyl-1,3,5-hexatriene (DPH) from Molecular Probes, and chloroform from Fisher Biotech. The cholesterol was recrystalized from ethanol before use. *Staphylococcus aureus* glutamyl endopeptidase (V8 protease) was obtained from ICN Biomedical, endoproteinase Lys-C (EKC) was obtained from Roche Molecular Biochemicals, and TPCK-treated trypsin was obtained from Worthington Biochemical.

Time-Resolved Photolabeling. The method was described in detail recently (*16*). Briefly, the system consisted of a conventional rapid mixing unit, a novel freeze-quenching unit, and a photolabeling unit. The freeze-quenching unit consists of a rotating metal disk, precooled in liquid nitrogen. nAChR-rich membranes (2 mg/mL final concentration in Ca^{2+} free TPS) were mixed (<0.5 ms) with [^{125}I]TID (4 μM final concentration), expelled onto the rotating disk, and frozen (<0.5 ms). Total incubation times had a functional lower limit of $\sim$1 ms. The frozen samples were irradiated at 366 nm with a model UVL-56 20 W Blak-Ray lamp (2 cm, 30 min) to photoincorporate the [^{125}I]TID into the membranes. Frozen samples were collected under red light with precooled forceps, placed in tared, precooled glass vials, and stored at −20 °C to await processing. With a designed total volume of TID/membranes of 1 mL, the maximum mass of nAChR-rich membranes obtainable from a single time-resolved photolabeling run was 2 mg of protein. Actual recoveries ranged from 25 to 75%, with recoveries at 2 ms usually nearer 25% (i.e., 0.5 mg). As this amount of nAChR-rich membranes was insufficient for analysis of labeled amino acids by Edman degradation, 3−4 runs at a single time-point were pooled to obtain sufficient mass for subsequent protein sequence analysis.

SDS−PAGE. Aliquots of the frozen [^{125}I]TID-labeled nAChR-membranes were analyzed for protein (micro-BCA protein assay, Pierce) and ^{125}I. The bulk of the frozen, [^{125}I]TID-labeled nAChR-membranes were thawed in appropriate amounts of 5× sample buffer such that the final solution contained 8% sucrose, 2% SDS, 0.4% glycerol, 0.0025% bromophenol blue, 0.36 M β-mercaptoethanol, and 0.06 M tris(hydroxymethyl)aminomethane (Tris), pH 6.8. The determined specific activities of the membrane suspensions (^{125}I cpm/μg of protein) were used to determine

[1] Abbreviations: TID, 3-(trifluoromethyl)-3-(*m*-iodophenyl) diazirine; nAChR, nicotinic acetylcholine receptor; TPS, *Torpedo* physiological saline; SDS, sodium dodecyl sulfate; PAGE, polyacrylamide gel electrophoresis; HPLC, high-pressure liquid chromatography; V8 protease, *Staphylococcus aureus* glutamyl endopeptidase; EKC, endoproteinase Lys-C; DOPC, 1,2-dioleoyl-phosphatidylcholine; DOPA, 1,2-dioleoyl-phosphate; Chol, cholesterol; EQ, equilibrium; DPH, diphenylhexatriene; TFA, trifluoroacetic acid; Tris, tris(hydroxymethyl)-aminomethane.

appropriate sample loading volumes for mass-balanced analytical SDS−PAGE and to determine the total mass loaded on preparative gels. nAChR subunits were resolved by SDS−PAGE using the Laemmli buffer system (*19*) with 8% acrylamide slab gels (1.5 mm thick) containing 0.32% bis-acrylamide. Following electrophoresis, polypeptides were visualized by Coomassie Blue stain, and bands containing the desired subunits were excised from the gel and soaked in distilled water for >30 min. Excised bands containing α-subunit were applied directly to a 24-cm, 15% acrylamide gel for *S. aureus* V8 protease mapping as described (*12*). For analytical V8 mapping gels, 10 μg of V8 protease (0.5 mg/mL) was used per sample, whereas, for preparative digests, 200 μg of V8 protease (0.5 mg/mL) was used per slab gel. V8 protease was applied in overlay buffer (5% sucrose, 0.1% SDS, 1 mM dithiothreitol, and 125 mM Tris-HCl, pH 6.8). EKC digests were fractionated on a 16.5% T/6% C tricine gel (*20*). Prestained low molecular mass standards (GIBCO-BRL) were used to determine approximate masses on tricine gels and for guidance in localizing nAChR-subunit fragments of interest from published digestion protocols (*7*). Excised bands were diced (1−2 mm), eluted passively (3 days) in 12 mL of elution buffer (100 mM NH_4HCO_3, 0.1% SDS, 2.5 mM dithiothreitol, pH 8.4), concentrated in Biomax 5K Ultrafree concentrators (Millipore), and either precipitated in 75% acetone (−20 °C) or separated directly by reversed-phase HPLC. Radiograms of the SDS−PAGE gels of [^{125}I]TID-labeled nAChR-rich membranes or subunit fragments were obtained using a Storm PhosphorImager (Molecular Dynamics) as described in ref *21*. In some cases, full-sized radiograms were used as templates to excise bands of interest from gels with low Coomassie Blue stain signal.

Enzymatic Digestion of [^{125}I]TID-Labeled nAChR-Subunits and Fragments. EKC digestions were performed in 15 mM Tris, 0.1% SDS, pH 8.1, for 1 week at 25 °C (*7*). Trypsin digestions were performed in 0.1 M NH_4CO_3, 0.1% SDS, 2% Genapol C-100, pH 7.8, for 3 days at 25 °C (*14*).

Reversed-Phase HPLC Purification of [^{125}I]TID-Labeled Fragments. Reversed-phase HPLC purification was performed on a Hewlett-Packard series 1100 HPLC with an inline degasser, column heater, and external absorbance and fluorescence detectors. Separations were achieved at 40 °C using a Brownlee Aquapore C-4 column (100 × 2.1 mm) with a C-2 guard column. Aqueous phase (solvent A) was 0.08% trifluoroacetic acid (TFA), and organic phase (solvent B) was 60% HPLC-grade acetonitrile, 40% HPLC-grade 2-propanol, 0.05% TFA. Flow rates were 0.2 mL/min, fractions were collected at 2.5-min intervals, and gradients are shown.

Amino-Terminal Sequence Analysis of [^{125}I]TID Labeled Fragments. Gas-phase amino-terminal sequence analysis was obtained on an Applied Biosystems 477A protein sequencer with an inline 120A analyzer. HPLC fractions of interest were loaded directly onto peptide supports (Beckman #290111) for sequencing (*22*). One-third of the product from each cycle was injected into the amino acid analyzer for residue identification and mass determination, while the remaining two-thirds was collected for ^{125}I measurement. Mass values were obtained from chromatographic peak heights and actual cpm and mass values are shown. Initial masses (I_o) and repetitive yields (R) were calculated from a nonlinear least-squares fit (Sigma Plot, Jandel Scientific) of the equation: $f(x) = I_o R^x$ where $f(x)$ is the mass of the amino acid in cycle x. Arginines, serines, histidines, tryptophans, and cysteines were excluded from the fit due to known problems with determining their masses. For quantification of [^{125}I]TID into subunit fragments, the cpm loaded onto the sequencing filter was divided by three times the calculated initial mass (I_o). For quantitation of [^{125}I]TID incorporation into specific residues, the background-subtracted ^{125}I cpm released at that cycle was divided by twice the mass of the amino acid calculated from the values of I_o and R.

Preparation of Lipid Vesicles. DOPC, DOPA, and Chol were solubilized in chloroform and mixed to give a composition of 55:12:33 molar ratio, respectively. The DPH in chloroform was added to the lipid mixture to give a final concentration of 1 mol %. The mixture was dried under a stream of nitrogen for 30 min, and residual solvent was removed under vacuum overnight. The solvent-free lipids were resuspended in TPS, vortexed, and freeze−thawed a minimum of 10 times using liquid nitrogen. Vesicles were prepared either by sonication under nitrogen for 1 h at 4 °C in a bath sonicator followed by a 5-min centrifugation (13600*g*) or by extrusion in a hand operated device (Avestin) fitted with polycarbonate filters (100-nm pores) through which the vesicles were passed ≥10 times. Vesicles prepared by either method gave identical results.

Analysis of [^{125}I]TID Photoincorporation into Lipids. After freeze-clamping and photolabeling, membrane samples were collected from the plate, made up to 4 mL with distilled water, and centrifuged for 10 min at 1300*g*, and the supernatant was discarded. The washing step was repeated using the same volume of distilled water. The pellet was vortexed for 2 min with 4 mL of a chloroform/methanol mixture (2:1). The organic phase was centrifuged for 30 min at 1300*g*. Aliquots of 0.4 and 0.1 mL of the organic phase were taken for organic phosphorus determination (*23*) and for analysis of ^{125}I, respectively. All samples were covered with aluminum foil and dried overnight in a drying rack at 110 °C.

Steady-State and Stopped-Flow Fluorescence Measurements. Steady-state measurements were made with a FloroMax 2 spectrofluorimeter (Jobin Yvon-Spex). The excitation spectrum (Em = 450 nm) of DPH in the lipid vesicles was recorded from 300 to 400 nm, and the emission spectrum (Ex = 360 nm) was recorded from 450 to 600 nm. Kinetic experiments were performed at 20 ± 4 °C with an Applied Photophysics BioSX-17 MV stopped-flow spectrofluorimeter with a deadtime of ∼1 ms. Equal volumes of various concentrations of DPH-labeled vesicles and of TID were rapidly mixed. The apparatus was thoroughly washed between experiments. DPH was excited at 360 nm with a 150 W Xe lamp, and emission was recorded at 450−480 nm (OMEGA 9525 interference filter) with data being collected on a logarithmic time base without electronic filtering. A minimum of five data sets were acquired and averaged to increase the signal-to-noise ratio. Traces were corrected by subtracting control data sets collected in the absence of TID. Corrected traces were fitted to exponential functions in IGOR (Wavemetrics) with further analysis being performed in KaleidaGraph (Abelbeck).

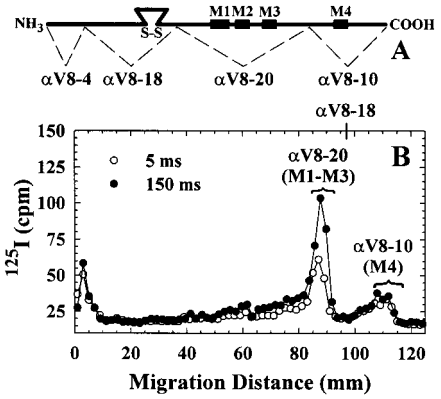

FIGURE 1: Incorporation of [^{125}I]TID into nAChR α-subunit fragments isolated from nAChRs labeled 5 and 150 ms after mixing. (A**)** Diagram of the primary structure of the *Torpedo* nAChR α-subunit illustrating the digestion pattern obtained from an *S. aureus* V8 protease mapping gel. (B**)** Comparison of the ^{125}I distribution in a V8 mapping gel of α-subunit from membranes which were frozen and photolabeled 5 ms (○) or 150 ms (●) after addition of [^{125}I]TID. nAChR-rich membranes (500 μL, 4 mg/mL) were mixed with an equal volume of [^{125}I]TID (8 μM), freeze-clamped, and photolyzed. Membrane aliquots (25 μg) were separated by SDS−PAGE (8% Laemmli), and the resulting gel was stained to visualize the nAChR subunits. The bands containing α-subunit were excised and placed on a mapping gel for digestion with V8 protease. The gel was stained and dried, and the individual lanes were cut into 2-mm slices for ^{125}I distribution determination. The mobilities of αV8−20, αV8−10, and αV8−18 (visualized by Coomassie Blue stain) are indicated.

RESULTS

In the resting state, [^{125}I]TID photoincorporates preferentially into amino acids in the M2 ion channel-lining domain (*13*) as well as into amino acids in the M3 and M4 lipid−protein interface domains (*14*, *15*). To determine which of these regions is responsible for the noncompetitive inhibition of the nAChR by TID, we determined the kinetics of [^{125}I]TID access to the M2 domain and to the lipid-interface by photolabeling nAChR-rich membranes flash frozen at defined times after mixing. We first characterized the distribution of [^{125}I]TID incorporation in the α-subunit within the four large fragments that can be produced by "in gel" digestion with V8 protease: fragments migrating at 20 kDa (αV8−20), 18 kDa (αV8−18), 10 kDa (αV8−10), and 4 kDa (αV8−4) (*12*). αV8−20 contains the membrane spanning segments M1−M3 including the M2 ion channel domain, whereas αV8−10 contains the M4 hydrophobic segment previously localized to the lipid−protein interface (Figure 1, panel A). For α-subunit obtained from nAChR-rich membranes freeze-clamped 5 or 150 ms after mixing with [^{125}I]TID and subsequently photolyzed, the incorporation of [^{125}I]TID within αV8−10 at 5 ms was 93% that seen at 150 ms. In contrast, [^{125}I]TID incorporation into αV8−20 at 5 ms was only 65% that of the 150 ms sample (Figure 1, panel B).

^{125}I Incorporation in nAChR α- and δ-Subunit Fragments. A preparative V8 protease mapping gel was used to isolate αV8−20 and αV8−10 from membranes photolabeled after freezing 2 ms after mixing or after 600 s (equilibrium or EQ). αV8−10 was digested with trypsin which was expected to produce a fragment beginning at the amino-terminus of αM4 (αV8−10T) (*14*). When the αV8−10 trypsin digests were purified by reversed-phase HPLC, the majority of the

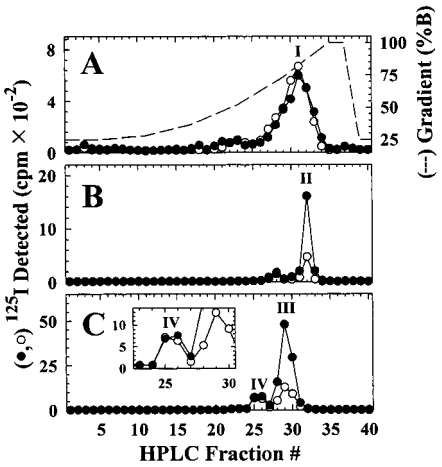

FIGURE 2: Reversed-phase HPLC separations of enzymatic digests of αV8−10 (A), αV8−20 (B), and δ-subunit (C). nAChR-rich membranes (500 μL, 4 mg/mL) were mixed with an equal volume of [^{125}I]TID (8 μM), aged for 2 ms (○) or 600 s (EQ, ●), freeze-quenched, and photolyzed. Three separate runs were performed for the 2-ms time point, and two runs were performed for the EQ time point. The labeled membranes for each time point were pooled, and individual subunits were separated by SDS−PAGE. After staining, the nAChR subunit bands were excised and the α-subunit bands were digested with V8 protease in a mapping gel. A radiograph of the wet mapping gel was obtained and used as a template to excise αV8−20 and αV8−10. These two bands along with the δ-subunit band from the primary gel were eluted and digested with either trypsin (αV8−10) or EKC (δ-subunit and αV8−20) as described in the methods section. The αV8−20 and δ-subunit EKC digests were separated by tricine SDS−PAGE. For each tricine gel, a 7−11-kDa band was excised and eluted (αEKC-8 and δEKC-10). Reversed-phase HPLC separations of these samples are shown: (A) Trypsin digest of αV8−10 (EQ, 3550 cpm injected, 3160 cpm recovered; 2 ms, 3600 cpm injected, 3150 cpm recovered); (B) αEKC-8 (EQ, 3440 cpm injected, 3030 cpm recovered; 2 ms, 1830 cpm injected, 1600 cpm recovered); and (C**)** δEKC-10 (EQ, 12 590 cpm injected, 11 860 cpm recovered; 2 ms, 4700 cpm injected, 4730 cpm recovered). Inset is an enlarged view of the region surrounding peak IV. Shown are the ^{125}I cpm (●, ○) and the HPLC gradient (- - -), which was the same for each chromatogram (solvent A, 0.08% TFA; solvent B, 60% acetonitrile, 40% 2-propanol, 0.05% TFA).

^{125}I-labeled material eluted in a broad distribution centered at ∼85% solvent B (Figure 2, panel A, peak I). For both time-points, fractions 30−32 were pooled and sequenced to identify and quantify peptides in each sample and to use that data to calculate the efficiency of photoincorporation (^{125}I cpm/pmol of peptide) at the respective time-points (αV8−10T, Table 1). Sequence analysis of fractions 30−32 from the EQ sample detected a single fragment beginning at αTyr-400 (I_o = 16 pmol). Sequence analysis of the corresponding fractions from the 2 ms sample detected a single fragment beginning at αGln-355 (I_o = 29 pmol), i.e., a trypsin cleavage site preceding αArg-399. (The reason for this variant cleavage pattern was not evident.) Therefore at 2 ms after mixing, the ^{125}I incorporation was 19 cpm/pmol in the αM4 containing fragment, while at 600 s, the ^{125}I incorporation increased to 31 cpm/pmol.

The αV8−20 fragment was digested with endoproteinase Lys-C (EKC), which is expected to produce an 8-kDa fragment beginning at the amino-terminus of αM2 (*7*). These digests were separated by tricine SDS−PAGE, and a band between 7 and 11 kDa (αEKC-8) was excised, eluted, and purified by reversed-phase HPLC (Figure 2, panel B). The majority of ^{125}I-labeled material eluted at about 90% solvent

Table 1: ^{125}I Incorporation into Subunit Fragments Isolated from nAChRs Labeled 2 ms after Mixing with [^{125}I]TID or at Equilibrium

sample	condition	fractions	^{125}I (cpm)	sequence	I_o (pmol)	cpm/pmol	ratio 2 ms/EQ
αV8−10T	2 ms	30−32	1670	αGln-355[a]	29	19	62% (αM4)
Figure 2A-I	EQ	30−32	1475	αTyr-400	16	31	
αEKC-8	2 ms	32	460	αMet-243	6.8	23	19% (αM2-M3)
Figure 2B-II	EQ	32	1600	αMet-243	4.6	116	
δEKC-10	2 ms	29	1280	δMet-256	18.7	23	17% (δM2-M3)
Figure 2C-III	EQ	29	4800	δMet-256	12.2	131	
δEKC-10	2 ms	25−26	1335	δAsn-200	7.0	31	44% (δM1)
Figure 2C-IV				δPhe-206	7.4		
	EQ	25−26	1425	δAsn-200	2.9	71	
				δPhe-206	3.8		

[a] The 2 ms αV8−10 trypsin digestion was incomplete, cause unknown.

B, centered at fraction 32 (Figure 2, panel B, peak II). Sequence analysis of αEKC-8 fraction 32 identified a single peptide beginning at αMet-243, the amino-terminus of αM2 (2 ms, I_o = 6.8 pmol; EQ, I_o = 4.6 pmol, Table 1). At 2 ms after mixing, the ^{125}I incorporation was 23 cpm/pmol in the fragment beginning at αMet-243, while at 600 s, the ^{125}I incorporation increased to 116 cpm/pmol.

The δ-subunit, isolated by SDS−PAGE from this same labeling experiment, was digested with EKC, which is expected to produce a 10-kDa fragment beginning at the amino-terminus of δM2 (*7*). The δ-subunit EKC digests were separated by tricine SDS−PAGE, and the region between 7 and 11 kDa (δEKC-10) was excised, eluted, and purified by reversed-phase HPLC (Figure 2, panel C). For the peak centered at fraction 29 (Figure 2, panel C, peak III), ^{125}I incorporation was much lower for the 2 ms sample than for the EQ labeling. An additional minor peak of ^{125}I was present in fractions 25 and 26 (Figure 2, panel C, peak IV and inset), which showed similar levels of ^{125}I for both the 2 ms and EQ labelings. Sequence analysis of δEKC-10 fraction 29 identified a single peptide beginning at δMet-256, the amino-terminus of δM2 (2 ms, I_o = 18.7 pmol; EQ, I_o = 12.2 pmol, Table 1). At 2 ms after mixing, the ^{125}I incorporation was 23 cpm/pmol in the fragment beginning at δMet-256, while at 600 s, the ^{125}I incorporation increased to 131 cpm/pmol. Sequence analysis of the pool of δEKC-10 fractions 25 and 26 identified two peptides beginning at δPhe-206 (2 ms, I_o = 7.4 pmol; EQ, I_o = 3.8 pmol) and δAsn-200 (2 ms, I_o = 7.0 pmol; EQ, I_o = 2.9 pmol, Table 1). Sequence analysis demonstrated that both fragments extend into δM1. At 2 ms after mixing, the ^{125}I incorporation was 31 cpm/pmol in the fragments containing δM1, while at 600 s, the ^{125}I incorporation increased to 71 cpm/pmol.

The Rate of Equilibration of [^{125}I]TID with δM2 and αM2. The ^{125}I release profiles from sequencing δEKC-10 fraction 29 (Figure 2, panel C) are shown in Figure 3, panel A, with data for 2 ms replotted in Figure 3, panel B, at an expanded scale to highlight the ^{125}I release profile. Prominent ^{125}I release was detected in cycle 9 (2 ms, 50 cpm; EQ, 360 cpm), consistent with incorporation at δLeu-265. The amount of ^{125}I cpm incorporated per picomole of δLeu-265 was 2.2 cpm/pmol at 2 ms and 28 cpm/pmol at EQ. Low level ^{125}I release was also detected in cycles 13 and 16 in both samples, consistent with incorporation at δVal-269 and δLeu-272. For δVal-269 and δLeu-272, the levels of ^{125}I incorporation at 2 ms were 0.6 and 0.3 cpm/pmol, which increased to 4.7 and 3.0 cpm/pmol at EQ, respectively.

The ^{125}I release profiles from sequencing αEKC-8 fraction 32 (Figure 2, panel B) are shown in Figure 3, panel C. For the EQ sample, low level ^{125}I release was detected in cycles 9 and 13, consistent with incorporation at αLeu-251 (3.2 cpm/pmol) and αVal-255 (5.5 cpm/pmol). Labeling of αLeu-251 and αVal-255 for the 2 ms sample was ≤20% that detected at EQ.

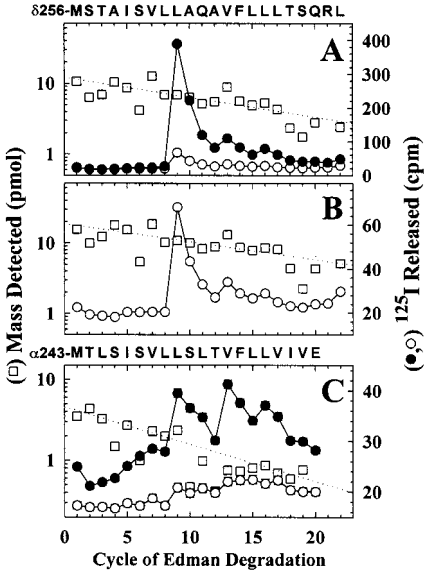

FIGURE 3: ^{125}I and mass released upon sequence analysis of M2 seqments from δ- and α-subunits. Subunit fragments were isolated from nAChRs labeled with [^{125}I]TID 2 ms after mixing or at equilibrium. (A) Sequence analyses of fraction 29 (Figure 2, panel C, peak III) from the HPLC purification of δEKC-10 (EQ, ●, 4800 cpm loaded, 2300 cpm left after 24 cycles of Edman degradation; 2 ms, ○, 1300 cpm loaded, 850 cpm left after 22 cycles of Edman degradation). A single peptide was detected that began at δMet-256, the amino-terminus of δM2 (□ in panel A (EQ): I_o = 12 ± 1 pmol, R = 94 ± 1%; □ in panel B (2 ms): I_o = 19 ± 1 pmol, R = 94 ± 1%). (B) Replot of the ^{125}I release profile of the 2 ms sample on an expanded scale. The primary peak of ^{125}I release in cycle 9 (2 ms, 48 cpm; EQ, 363 cpm) corresponded to δLeu-264 within δM2. The ^{125}I cpm/pmol of residue for the 2 ms and EQ samples at δLeu-265 were 2.2 and 27.5, respectively. There was also lower level ^{125}I release at both time points in cycle 13 (δVal-268, 2 ms, 0.6 cpm/pmol; EQ, 5 cpm/pmol) and cycle 16 (δLeu-271, 2 ms, 0.3 cpm/pmol; EQ, 3 cpm/pmol). (C) Sequence analyses of fraction 32 (Figure 2, panel B, peak II) from the HPLC purification of αEKC-8 (EQ, ●, 1600 cpm loaded, 830 cpm left after 20 cycles of Edman degradation; 2 ms, ○, 460 cpm loaded, 340 cpm left after 20 cycles of Edman degradation). A single peptide was detected that began at αMet-243, the amino-terminus of αM2 (□, (EQ): I_o = 4.6 ± 0.3 pmol, R = 90 ± 1%; (2 ms): I_o = 6.8 ± 0.4 pmol, R = 90 ± 1%, data note shown). Low level ^{125}I release occurred in cycle 9 (αLeu-251, 2 ms, 0.7 cpm/pmol; EQ, 3 cpm/pmol) and cycle 13 (αVal-255, 2 ms, 0.6 cpm/pmol; EQ, 6 cpm/pmol).

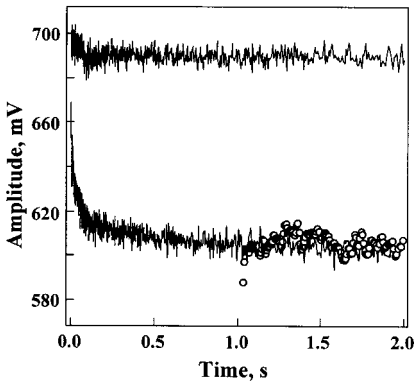

FIGURE 4: Rate of equilibration of TID with the lipid bilayer. Lipid vesicles (DOPC/DOPA/Chol 55:12:33 mol %) doped with one mole percent DPH were rapidly mixed with TID and the fluorescence intensity was monitored against time as described in the text. The voltage offset is arbitrary. The averaged traces from five shots are shown in the continuous traces. The final lipid concentration in all traces is 25 μM. The final TID concentration is zero in the upper trace and 10 μM in the others. The circles are from a single shot in which the lamp was shuttered during the first second. The first few points represent the shutter artifact.

The Rate of Equilibration of TID with Lipid Bilayers. Under equilibrium conditions, addition of TID to DOPC/DOPA/Chol (55:12:33 molar ratio) lipid vesicles (10 μM in lipid) doped with 1% mole DPH caused the intensities of the steady-state excitation and emission spectra of DPH to decrease but caused no shift in the wavelengths of the major peaks. For example, at the emission maximum, 10 μM TID caused a 70% decrease in intensity.

Figure 4 shows typical uncorrected traces under stopped flow conditions. In the absence of TID, the fluorescence signal from DPH in 25 μM lipid varied little with time. However, when these vesicles were mixed with 10 μM TID (final concentrations), the recorded fluorescence intensity decreased rapidly from around 690 to 645 mV in 5 ms and then more slowly to about 600 mV at 1 s. To control for possible photolysis of TID in the observation cuvette, parallel identical experiments were performed in which the xenon lamp was shuttered during mixing and for a short time thereafter. In the example in Figure 4, the lamp was shuttered for the first second of the trace, but the signal had nonetheless decreased ~90 mV in the dark. Indeed, it was superimposable with the trace obtained without shuttering over the full recording time of 10 s. Thus, photolysis appears negligible on this time scale.

Stopped flow traces with TID could be fit to two exponentials of approximately equal amplitude under all conditions. The faster process had a rate of ~100−1000 s^{-1}, depending on lipid concentration, and the slower process had a rate of ~18 s^{-1}, which did not vary with lipid or TID concentration. The absolute amplitudes of both processes increased with lipid and TID concentration, but their fractional amplitudes remained constant. In the absence of TID, only the slow rate was seen, although its amplitude was very small. Because the slower process contributed little amplitude in the first few milliseconds, which was the main region of interest in this study, and because it occurred in the absence of TID, it was not investigated further.

The kinetics of the quench of DPH fluorescence by TID were studied both as a function of lipid concentration (2.5−250 μM) at fixed TID concentration (10 μM) and as a function of TID concentration (1−10 μM) at fixed lipid concentration (20 μM; all concentrations given are post-mixing). The minimum lipid concentration limit was determined by the loss of detectable quenching (10 mV), whereas the maximum lipid concentration limit was determined by light scattering artifacts. The maximum TID concentration examined was limited by its solubility in buffer, whereas the minimum was limited by signal considerations.

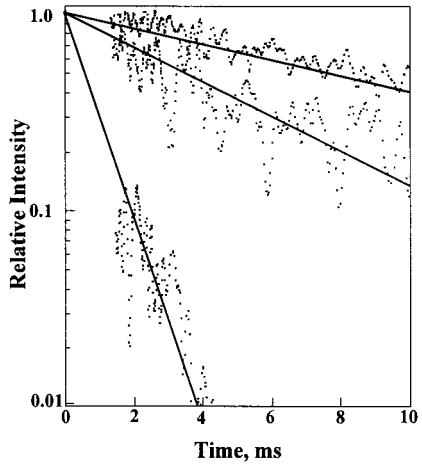

FIGURE 5: Dependence of the rate of equilibration with TID on the lipid concentration. Averaged data with lipid-only controls subtracted (see Materials and Methods) were normalized to the equilibrium value by the transform $[1 - (F(t)/F(\text{inf})]$ where, $F(t)$ and $F(\text{inf})$ are the fluorescence intensity at time t and at equilibrium, respectively. The slope of the lines are the negative of the first-order rate constant. The final TID concentration was 10 μM in all traces. The final lipid concentration and the rate constant are from top to bottom: 10 μM and 93 ± 5 s^{-1}, 20 μM and 200 ± 13 s^{-1}, 250 μM and 1250 ± 25 s^{-1}.

At a fixed final concentration of 10 μM TID, the initial rate of quenching varied from 96 ± 7 s^{-1} at 2.5 μM lipid to 203 ± 9 s^{-1} at 25 μM lipid, and the amplitude quenched varied nearly linearly from 10.0 ± 0.2 mV to 68 ± 1 mV. At the higher lipid concentrations both light scattering and the rapidity of the kinetics made quantitative work difficult. However, to better mimic photolabeling conditions, we conducted one semiquantitative study at 250 μM lipid. At this concentration, much of the quenching occurred during the deadtime of the stopped flow spectrometer making it difficult to fit the untransformed data. Instead the data between 1 and 4 ms were linearized to $[1 - (F(t)/F_{\text{inf}})]$, where $F(t)$ is the fluorescence intensity at time t, and F_{inf} is the fluorescence intensity at equilibrium, and fitted to a linear function through the origin. This analysis is shown in Figure 5 together with data obtained at 10 and 20 μM lipid for comparison. The scatter in the data can be seen to increase with lipid concentration especially at short times. At 250 μM lipid, quenching is about 80% complete in the first millisecond (an absolute change of ~250 mV), and the rate constant can be estimated from the linear fit to be 1250 s^{-1}. This estimate is subject to large systematic errors because of the small fraction of the signal available for fitting.

At a fixed final concentration of 20 μM lipid, the initial rate was essentially constant at ~200 s^{-1} between 1 and 10 μM TID and the amplitude of quenching increased from 23 to 60 mV.

Kinetic Analysis of DPH Quenching Data. The data were analyzed according to a bimolecular scheme with the

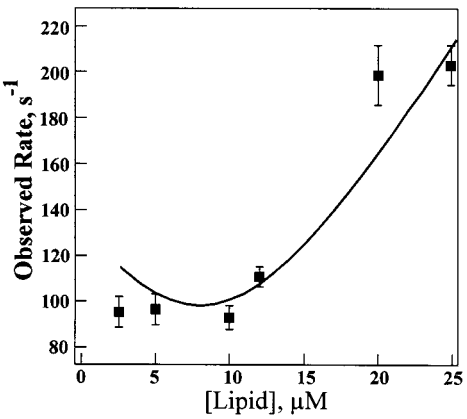

FIGURE 6: Observed rate of dissolution of TID into lipid bilayers is consistent with a second-order kinetics model. Data are shown as mean ± standard deviation. The line is the nonlinear least-squares fit of the data to eq 1 with rate constants $k_f = 1.1 \pm 0.2 \times 10^7$ M^{-1} s^{-1} and $k_r = 22 \pm 8$ s^{-1}. See text for details.

assumption that the rate-determining step is the reversible dissolution of TID in the lipid bilayer. The partition coefficient of TID in *Torpedo* nAChR-rich membranes is ~10^5 (*12*), so the high concentration of TID in the bilayer will ensure that the collision rate with DPH is not rate limiting. Following the analysis that Bradrick et al. (*24*) developed to analyze the kinetics of melittin−lipid interactions, the dependence of the observed rate, k_{obs}, on the initial concentrations of TID, $[TID]_o$, and lipid, $[L]_o$, is given by eq 1:

$$k_{obs} = \{(k_r + k_f([L]_o + [TID]_o))^2 - 4k_f^2[L]_o[TID]_o\}^{0.5} \quad (1)$$

where k_f is the bimolecular rate constant for TID entering the bilayer and k_r is the unimolecular rate constant for TID leaving the bilayer. The results of the analysis of k_{obs} as a function of lipid concentrations from 2.5 to 25 μM are shown in Figure 6. The model is consistent with the initial lack of dependence of k_{obs} on lipid concentration, followed by an increase when $[L]_o > [TID]_o$. Nonlinear least-squares fits of the data generated rate constants of $k_f = 1.1 \pm 0.2 \times 10^7$ M^{-1} s^{-1} and $k_r = 22 \pm 8$ s^{-1}. These values produce an equilibrium constant of 5×10^5 M^{-1}.

Rate of Equilibration of [^{125}I]TID with Phospholipids. Three separate photolabeling experiments were performed under standard conditions (final concentrations where 2 mg/mL protein and 4 μM [^{125}I]TID) with preincubation times of 1 and 10 ms. The standard deviations within experiments were in the range of 10−20% of the mean. Photoincorporation into the lipid extract did not differ between 1 and 10 ms. For example, in one experiment with four samples at each time point, the photoincorporation was, at 1 ms, 4400 ± 740, and at 10 ms, 4200 ± 600 (cpm/nmol phosphorus ± standard deviation).

DISCUSSION

The focus of this study was to understand the mechanism of resting state inhibition of agonist-induced cation flux by TID. Previous work had demonstrated that TID partitions extensively into the lipid of nAChR-rich membranes and that it photoincorporates both at the lipid−protein interface in hydrophobic segments M1, M3, and M4 and into a site in the lumen of the channel (M2) (*12*, *14*, *15*). Agonist-induced cation flux studies have shown that resting state inhibition develops at a rate of about 10 s^{-1} (*10*), and time-resolved photolabeling of TID into subunits has demonstrated that equilibration occurs in two phases, one reaching completion in a few milliseconds and the other at a rate comparable to resting state inhibition (*16*). To characterize the amino acid residues accessed during these two time domains, our strategy was to compare the labeling pattern at incubation times corresponding approximately to the completion of the fast and slow phases. The times chosen were 2 ms and 600 s, respectively (Table 1).

When TID is rapidly mixed with nAChR-rich membranes, much of it is transferred from the buffer to the membrane. How large is this effect, and does it occur on a time scale that might complicate interpretation of the kinetics of equilibration with the nAChR? An experimental estimate of the TID lipid/buffer partition coefficient in nAChR-rich membranes is ~10^5 (*12*). The final total concentrations after mixing are 2 mg/mL membranes and 4 μM TID. From these values, one can estimate that during equilibration the aqueous TID concentration drops nearly 100-fold to ~50 nM, while the concentration of TID in the bilayer rises to ~4 mM, and the majority of the TID (>99%) ends up in the membranes. To estimate how rapidly this vast redistribution occurs, we adopted two strategies. First, we determined the rate of dissolution of TID into a simple lipid bilayer whose composition was chosen to mimic that of *Torpedo* vesicles, and second, we determined the degree of photoincorporation into the lipids of nAChR-rich membranes using time-resolved photolabeling.

At the membrane concentration under which photolabeling was carried out (~1.25 mM lipid), light scattering was too severe to study the fluorescence quenching of DPH by TID. However, a systematic study of the kinetic quenching at lower lipid bilayer concentrations (≤25 μM DOPC/DOPA/Chol bilayers) allowed us to establish the rate constants for a bimolecular kinetic model. Extrapolating to the conditions used for photolabeling (4 μM TID, ~1.5 mM lipid), the model predicts a k_{obs} of 14 ± 2.5 ms^{-1}. Thus, the lipid bilayer would be equilibrated with TID within ~250 μs, well within the dead time of our time-resolved photolabeling apparatus. This theoretical extrapolation is consistent with the fact that 80% equilibration was observed at 1 ms at 6 times lower lipid concentration (250 μM, Figure 5). Because of complications arising from intrinsic fluorescence, similar experiments were not carried out in nAChR vesicles, and one cannot rule out the possibility that access to that membrane's lipid might be hindered relative to that of a protein-free bilayer. Therefore, we also examined the rate of equilibration with the lipids in intact nAChR-rich membranes under the same conditions as used for time-resolved photolabeling of the receptor. These experiments showed that incorporation per mole of phospholipid was independent of preincubation time between 1 and 10 ms. Thus TID equilibrates with the nAChR membrane's lipids in less than a millisecond.

Overall, these experiments allow us to conclude that before the nAChR-rich membrane suspensions are freeze-quenched, TID has completely equilibrated between the bulk phases even after the shortest preincubations used in this work.

The Rate of Equilibration with the Lipid−Protein Interface. The αV8−10 proteolytic fragment, and the correspond-

ing fragments from the other nAChR subunits, contain a large portion of the major cytoplasmic loop as well as the M4 hydrophobic segments (Figure 1, panel A). However, prior work has established that [^{125}I]TID incorporates only into residues that are in the M4 hydrophobic segments (*15*). In one of our experiments with αV8−10 fragments, photoincorporation had reached 93% of that at equilibrium after 5 ms of preincubation (Figure 1), while in another it had reached 62% at 2 ms (Table 1). The observation that residues in the lipid−protein interface continue to equilibrate with TID for a few milliseconds after equilibration with lipid is complete suggests that TID's access to the protein surface within the lipid may be somewhat sterically hindered.

Rate of TID Equilibration Within the Ion Channel. After 2 ms of preincubation, photoincorporation into proteolytic fragments containing the M2 and M3 segments was only ∼20% the equilibrium incorporation (αEKC-8 and δEKC-10, Table 1). Sequence analysis revealed that three residues that face into the ion channel on three successive turns of the δM2 helix were labeled by [^{125}I]TID both at 2 ms and at equilibrium, with the incorporation at 2 ms averaging only $10 \pm 2.5\%$ the incorporation at equilibrium (Figures 3, panels A and B). These labeled residues, numbered 9′, 13′, and 16′ from the conserved positive charge at the amino-terminal end of the M2 segment, were δLeu-265, δVal-269, and δLeu-272, respectively. The relative degree of incorporation of [^{125}I]TID after a preincubation of only 2 ms at these three residues was 7:2:1, and this pattern remained essentially unchanged at equilibrium. Although more difficult to quantify, homologous residues in αM2 were labeled in a similar manner (Figure 3, panel C). These results suggest that the level of incorporation increased with the same kinetics in each of the three residues and that, whatever the restricted pathway along which TID gains access to its binding pocket, there is no significant potential energy minimum for TID−protein interactions in this region other than the pocket bounded by the three residues labeled.

The labor involved discouraged us from following the detailed kinetics at the residue level. However, it is clear that after the first few milliseconds, increasing incorporation of [^{125}I]TID occurs into the M2 channel lining residues and not into the M4 segment. Our previous study of time-resolved incorporation of TID into nAChR was carried out at many more time points but only at the subunit level (*16*). The current results are quite consistent with those more detailed kinetics. At the subunit level, about half of the equilibrium level of photoincorporation was seen for membranes frozen within 2 ms, a result paralleling TID equilibration at the lipid−protein interface in the present study. The remainder of the incorporation increased at a rate, in the δ-subunit, of $14 \pm 4\ s^{-1}$, which is quite consistent with the 10% occupancy of the site in the M2 ion channel domain at 2 ms observed in this study. Thus, we can conclude that TID binding within the ion channel, which is lined by the identified M2 residues, equilibrates at a rate of $\sim 10\ s^{-1}$.

Site of Resting State Inhibition. Wu et al. (*10*) carried out quenched-flow flux experiments that showed that TID was a resting state inhibitor of the agonist-induced flux in *Torpedo* vesicles. When TID was added simultaneously with agonist and cation flux was measured over a few milliseconds, no inhibition was observed, although longer preincubations with TID did produce progressively more inhibition. At 18 °C, for example, preincubation with 10 μM TID for ∼100 ms was required to cause complete inhibition of flux and the observed rate constant for TID inhibition was $20\ s^{-1}$. Their inhibition curves had Hill coefficients of one from which they concluded that inhibition could occur either at a single site (i.e., within the ion channel) or at a number of sites of equal affinity, such as might occur at the lipid−protein interface. Our present data show that the ion channel is the only labeled region with slow enough access kinetics to be the site of resting state inhibition. We cannot, however, rule out the possibility that TID's rapid equilibration with the lipid and/or lipid−protein interface plays a role in enhancing access to the channel pore.

Our studies determine the kinetics of equilibration of [^{125}I]TID with the *Torpedo* nAChR ion channel in the closed state. In a recent study using electrophysiological techniques to characterize the kinetics of TID inhibition of fetal mouse nAChRs expressed in Xenopus oocytes, Forman (*11*) demonstrated two components of inhibition: one consistent with resting state inhibition, occurring at a rate comparable to that in *Torpedo*, and a second consistent with open channel block, occurring only after preincubation with TID. It is difficult at this time to relate the latter result to our study, because there are significant, quantitative differences between the kinetics of gating of mouse and *Torpedo* nAChRs by ACh, and there are also differences in the structure of the ion channel domains that affect the state selectivity of drugs binding in the ion channel. However, future studies of [^{125}I]TID time-resolved photolabeling during agonist-stimulated gating will define the kinetics of [^{125}I]TID binding within the *Torpedo* nAChR ion channel in the open state.

ACKNOWLEDGMENT

We thank Dr. S. Shaukat Husain for synthesizing TID.

REFERENCES

1. LeNovere, N., Corringer, P. J., and Changeux, J. P. (1999) *Biophys. J. 76*, 2329−2345.
2. Miyazawa, A., Fujiyoshi, Y., Stowell, M., and Unwin, N. (1999) *J. Mol. Biol. 288*, 765−786.
3. Hucho, F., Tsetlin, V. I., and Machold, J. (1996) *Eur. J. Biochem. 239*, 539−557.
4. Corringer, P.-J., Le Novere, N., and Changeux, J.-P. (2000) *Annu. Rev. Pharmacol. Toxicol. 40*, 431−458.
5. Prince, R. J., and Sine, S. M. (1998) in *The Nicotinic Acetylcholine Receptor: Current Views and Future Trends* (Barrantes, F. J., Ed.) pp 31−59, Springer-Verlag and R. G. Landes Company, Austin, TX.
6. Arias, H. R. (1998) *Biochim. Biophys. Acta 1376*, 173−220.
7. Gallagher, M. J., and Cohen, J. B. (1999) *Mol. Pharmacol. 56*, 300−307.
8. Middleton, R. E., Strnad, N. P., and Cohen, J. B. (1999) *Mol. Pharmacol. 56*, 290−299.
9. White, B. H., Howard, S., Cohen, S. G., and Cohen, J. B. (1991) *J. Biol. Chem. 266*, 21595−21607.
10. Wu, G., Raines, D. E., and Miller, K. W. (1994) *Biochemistry 33*, 15375−15381.
11. Forman, S. A. (1999) *Biochemistry 38*, 14559−14564.
12. White, B. H., and Cohen, J. B. (1988) *Biochemistry 27*, 8741−8751.
13. White, B. H., and Cohen, J. B. (1992) *J. Biol. Chem. 267*, 15770−15783.
14. Blanton, M. P., and Cohen, J. B. (1992) *Biochemistry 31*, 3738−3750.
15. Blanton, M. P., and Cohen, J. B. (1994) *Biochemistry 33*, 2859−2872.

16. Addona, G. H., Kloczewiak, M. A., and Miller, K. W. (1999) *Anal. Biochem. 267*, 135−140.
17. Chiara, D. C., and Cohen, J. B. (1997) *J. Biol. Chem. 272*, 32940−32950.
18. Brunner, J., and Semenza, G. (1981) *Biochemistry 20*, 7174−7182.
19. Laemmli, U. K. (1970) *Nature 227*, 680−685.
20. Schägger, H., and von Jagow, G. (1987) *Anal. Biochem. 166*, 368−379.
21. Johnston, R. F., Pickett, S. C., and Barker, D. L. (1990) *Electrophoresis 11*, 355−360.
22. Pedersen, S. E., Sharp, S. D., Liu, W.-S., and Cohen, J. B. (1992) *J. Biol. Chem. 267*, 10489−10499.
23. McClare, M. R. (1971) *Anal. Biochem. 39*, 527−530.
24. Bradrick, T. D., Philippetis, A., and Georghiou, S. (1995) *Biophys. J. 69*, 1999−2010.

BI0021481